



Identification of doxorubicin as a potential therapeutic against SARS-CoV-2 (COVID-19) protease: a molecular docking and dynamics simulation studies

Qazi Mohammad Sajid Jamal^a , Ali H. Alharbi^a  and Varish Ahmad^b 

^aDepartment of Health Informatics, College of Public Health and Health Informatics, Qassim University, Al Bukayriyah, Saudi Arabia; ^bHealth Information Technology Department, Faculty of Applied Studies, King Abdulaziz University, Jeddah, Kingdom of Saudi Arabia

Communicated by Ramaswamy H. Sarma

ABSTRACT

After one year, the COVID-19 pandemic caused by SARS-CoV-2 is still the largest concern for the scientific community. Of the many recognized drug targets of SARS-CoV-2, the main protease is one of the most important target due to its function in viral replication. We conducted an in silico study with repurposing drugs of antibiotics class against virus protease and peptidase using AutoDock tool. The following significant binding energy interaction was observed with protease (PDB: 6LU7) like piperacillin -7.25; tobramycin -9.20 and doxorubicin (Doxo) -10.04 kcal/mol and with peptidase (PDB: 2GTB) piperacillin -7.08; tobramycin -8.54 and Doxo -9.89 kcal/mol. Furthermore, the interaction and stability behavior of the Doxo-protease and Doxo-peptidase complexes were analyzed for a 100-nanosecond (ns) time. Calculated RMSD values observed using molecular dynamics simulation (MDS) were found to be 0.15–0.25 nm, RMSF calculation per residues showed a value near 0.2 nm and R_g values remained approximately 2.25 nm. MM-PBSA analysis of total binding energy calculation of Doxo-protease and Doxo-peptidase complexes are found to be -148.692 and -105.367 kJ/mol, respectively. Moreover, amino acid residue ASP-197 showed the lowest contribution binding energy i.e. -18.1185 kJ/mol, and amino acid residue ASP-187 showed -17.0267 kJ/mol contribution energy. Thus, significant docking interaction and stable dynamicity of Doxo-protease complex with time was suggested that Doxo could be a choice to inhibit potentially the viral proteases that could prevent the entry inside the host cell to control the COVID-19 disease.

Abbreviations: Å: Angstrom; Doxo: Doxorubicin; kcal/mol: kilocalories per mole; kJ/mol: kilo joule per mole; μ M: micro molar; nm: nanometer; ns: nanoseconds; ps: picoseconds

ARTICLE HISTORY

Received 21 June 2020
Accepted 15 March 2021

KEYWORDS

SARS-CoV-2; Doxorubicin; antiviral drugs; protease inhibitor; MDS

1. Introduction

Recently, the population of the world has encountered a challenge from a dangerous risk named severe acute respiratory syndrome coronavirus 2 (SARS-CoV-2), which is popularly known as Coronavirus Disease 2019 (COVID-19) (Paraskevis et al., 2020). The disease is caused by a member of genera β -*Coronaviridae* which is later described as an RNA virus (Pal et al., 2020; WHO, 2008). WHO released data on COVID-19, as on 14 May 2020 that 4,179,479 infected persons and 287,525 human deaths have been confirmed worldwide in 215 countries (<https://www.who.int/emergencies/diseases/novel-coronavirus-2019/situation-report>). The different infected persons have been recorded from different countries with a prompt rate of transmission of disease (Khaerunnisa et al., 2020).

The disease is characterized by sore throat, cough, headache, myalgia, fatigue, fever and breathlessness (Lovato et al., 2020). In 2003, the SARS-CoV came into scientist knowledge which has been reported with a much higher mortality rate (12%) and infected more the 8098 persons across 26 countries.

The COVID-19 has been reported with less (9%) mortality rate than the SRAS-CoV (2003) (Shereen et al., 2020).

The incubation of the disease is 1–14 days and after 6–7 days, the disease can progress to pneumonia, complexes and even death also. The health complication is due to extreme release of Interleukin (IL) such as IL-10, IL7, IL2, macrophage inflammatory protein 1A, monocyte chemoattractant protein 1, inducible protein 10, granulocyte-macrophage colony-stimulating factor and tumor necrosis factor (Huang et al., 2020). Moreover, many cases of asymptomatic or no fever have been reported (Lu et al., 2021).

It has also been reported that a high level of creatinine, prothrombin time, Lactate dehydrogenase (LDH), Alanine transaminase (ALT)/Aspartate transaminase (AST), and Creatine kinase (CPK) are associated with severe conditions of disease. The patients are diagnosed with molecular and immunological tests using respiratory samples like sputum/throat swab/bronchoalveolar lavage/and endotracheal aspirates (Abbasi-Oshaghi et al., 2020). Imaging technologies like X-ray and CT scans have also been used in the preliminary examination of the disease conditions (Singhal, 2020).

Currently, there is no well-tested treatment method discovered yet to control the disease CoV. For the progress of significant treatment against this disease, the targeting active sites or ligand interacting proteins must be explored for therapeutic purpose. Currently, the genome of the virus COVID-19 and probable cell-interacting protein have been explored, which will be helpful in the designing of the therapeutic intervention for the control of the disease. Many phytoconstituents, previously used FDA-approved drugs, including antiviral drugs have been tested against this virus (Zhou et al., 2020).

Many therapeutics molecules have been used for the management of different kinds of diseases. The therapeutics uses of herbal medicines, chemical entities, antibiotics, anti-fungal antiviral, anticoagulant, therapeutics proteins and vaccines are well explored. Antimalarial drug Artemisinin from the herb *Artemisia annua* (Pan et al., 2013), antibacterial and antifungal Withafarin A recovered from *Withania somniferum*, polyacetylene active against bacteria, fungi and virus have been reported from *Arctium lappa* (Cowan, 1999). Moreover, monoclonal antibodies such as adalimumab (Humira) have been well explored for the treatment of various cancers (Lu et al., 2020). Each drug has a different mechanism of action such as beta-lactam antibiotics including penicillin (PCNs), carbapenems monobactam (Aztreonam) and cephalosporins inhibit cell wall synthesis, Macrolides – erythromycin, azithromycin, and clarithromycin inhibit protein synthesis through binding with 50S ribosomal, while tetracyclines – tetracycline, doxycycline, and minocycline act as 30S ribosomal bacterial protein synthesis inhibitors, aminoglycosides like tobramycin, streptomycin, amikacin, and gentamicin also inhibit protein synthesis mediated by 30S ribosomes.

The role of viral proteins (spike protein, protease and peptidase) in the pathogenesis of COVID-19 disease is well reported. Ribosomes mainly 30S and 50S units are universal translational machinery of the living cells involved in protein synthesis. The selected repressor drugs of this study bind to 30S or 50S ribosomal units, inhibit protein synthesis and mediate their antimicrobial effect. More negative docking energies of these drugs observed with protease and peptidase of viral enzymes showing the significant binding interaction with the viral enzymatic proteins. Moreover, the dynamics simulation study of these drugs with studied target enzymes is found to be significant and could interfere with the viral pathogenesis.

Fluoroquinolones including ciprofloxacin, ofloxacin, gatifloxacin inhibit DNA gyrase as well as topoisomerase (Zumla et al., 2016). The Coronavirus is an RNA virus, and antiviral drugs commonly inhibit reverse transcriptase like zidovudine, stavudine, zalcitabine, lamivudine, abacavir, tenofovir, didanosine and emtricitabine (Yan et al., 2020). The genome of virus SARS-CoV synthesize many proteins by the gene expression of replicase which is an important segment of the CoV genome expressed proteases for the release of 16 non structural proteins (NSPs) namely polyprotein PP1a/PP1ab. The enzyme chymotrypsin-like main proteases (M^{pro}) belong to cysteine protease, cleaves the C-terminal part of the enzyme, whereas PLpro papain-like protease possessed N-

terminal part of the enzyme and these could be a target to control the virus infection (Barretto et al., 2005; Lindner et al., 2005; Ullrich & Nitsche, 2020).

The in silico screening studies have been conducted and signified the interaction COVID-19 target molecules. Moreover, scientific efforts are being contributed for the search for effective treatment of COVID-19 disease but to date, no effective molecules are available to control the virus. Also, molecular dynamics simulations (MDS) are one of the emerging computational tools to study the time-dependent behavior of molecules in a biological system. Protein and nucleic acids are key biomolecules of the cells that regulate most of the life-supporting processing of the cell. Biological molecules such as protein, DNA or RNA produce responses through a complex process and changes dynamically with time as the responses proceed. Thus, molecules behave differently with different molecules of the cellular environment and result in disease conditions and pathological conditions. Moreover, cell surfaces including extracellular molecules as well as internal molecules of extra cellular matrix (ECM) have also been reported to behave differently in the presence of therapeutics or drug molecules being prescribed to manage the disease condition (Ahmad, 2020).

Thus, in search of a new drug molecule, in this study, we conducted the computational-based studies of the different class of antibiotics with the COVID-19 viral protease and peptidase proteins and validated the best complex through MDS (Barretto et al., 2005).

2. Material and methods

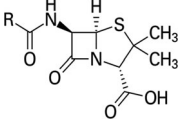
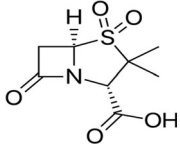
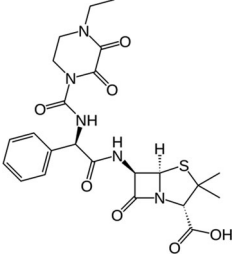
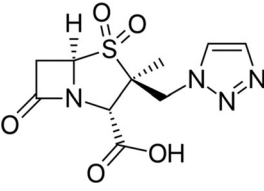
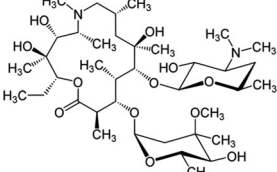
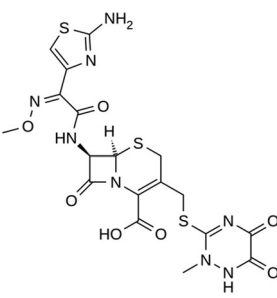
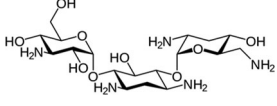
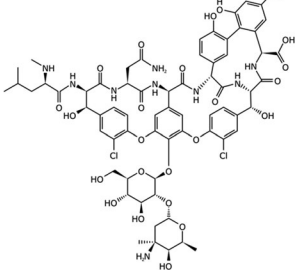
2.1. Drug compounds preparation

The two-dimensional (2D) structures of drug compounds penicillin, sulbactam, piperacillin, tazobactam, azithromycin, ceftriaxone, tobramycin, vancomycin, trimethoprim, doxorubicin (Doxo) and artemisinin (Table 1) were downloaded from PubChem Database provided by National Center for Biotechnology Information (NCBI) (<https://pubchem.ncbi.nlm.nih.gov/>). The 2D drug compounds chemical structure cannot be used directly to run docking studies it should be further converted to .pdb files using CORINA online three-dimensional (3D) structure generator (https://www.mn-am.com/online_demos/corina_demo) after providing drug compounds SMILES IDs as an input and further energy minimization was done after implementing CHARMM forcefield (Brooks et al., 2009) available in Discovery Studio visualizer 2019 (Biovia et al., 2000).

2.2. COVID-19 receptor molecules preparation

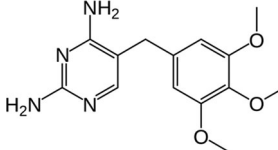
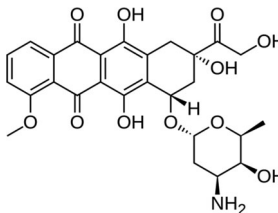
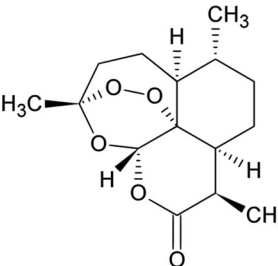
We have downloaded the crystal 3D structures of COVID-19 Protease (PDB: 6LU7) (Figure 1(a)) bounded with N3 inhibitor and COVID-19 main peptidase (PDB: 2GTB) (Figure 1(b)) bounded with substrate-like aza-peptide epoxide from Protein Data Bank (PDB) (www.rcsb.org) (Berman et al., 2000). To prepare the downloaded 3D crystal structure for docking studies, we have removed the water molecules and HETATM

Table 1. Detailed information of selected drugs for the molecular interaction analysis.

S.No	Drug name	Molecular formula	Molecular weight	Structure	SMILES ID	PubChem ID
1	Penicillin	C ₁₆ H ₁₈ N ₂ O ₄ S	334.4 g/mol		<chem>CC1(C(N2C(S1)C(C2=O)NC(=O)CC3=CC=CC=C3)C(=O)O)C</chem>	CID:2349
2	Sulbactam	C ₈ H ₁₁ NO ₅ S	233.24 g/mol		<chem>CC1(C(N2C(S1(=O)=O)CC2=O)C(=O)O)C</chem>	CID:130313
3	Piperacillin	C ₂₃ H ₂₇ N ₅ O ₇ S	517.6 g/mol		<chem>CCN1CCN(C(=O)C1=O)C(=O)NC(C2=CC=CC=C2)C(=O)NC3C4N(C3=O)C(C(S4)C)C(=O)O</chem>	CID:43672
4	Tazobactam	C ₁₀ H ₁₂ N ₄ O ₅ S	300.29 g/mol		<chem>CC1(C(N2C(S1(=O)=O)CC2=O)C(=O)O)CN3C=CN=N3</chem>	CID:123630
5	Azithromycin	C ₃₈ H ₇₂ N ₂ O ₁₂	749 g/mol		<chem>CCC1C(C(C(N(CC(CC(C(C(C(C(=O)O)1)C)OC2CC(C(C(O2)C)O)(C)OC)OC3C(C(C(O3)C)N(C)C)O)(C)O)C)C)O)(C)O</chem>	CID:447043
6	Ceftriaxone	C ₁₈ H ₁₈ N ₈ O ₇ S ₃	554.6 g/mol		<chem>CN1C(=NC(=O)C(=O)N1)SCC2=C(N3C(C(C3=O)NC(=O)C(=NOC)C4=CSC(=N4)N)SC2)C(=O)O</chem>	CID: 5479530
7	Tobramycin	C ₁₈ H ₃₇ N ₅ O ₉	467.5 g/mol		<chem>C1C(C(C(C1N)OC2C(C(C(C(O2)CO)N)O)O)OC3C(CC(C(O3)CN)O)N</chem>	CID:36294
8	Vancomycin	C ₆₆ H ₇₅ Cl ₂ N ₉ O ₂₄	1449.2 g/mol		<chem>CC1C(C(CC(O1)OC2C(C(C(OC2OC3=C4C=C5C=C3OC6=C(C=C(C(C=C6)C)C(C(=O)NC5C(=O)NC7C8=CC(=C(C=C8)O)C9=C(C=C(C=C9)O)C(NC(=O)C(C1=CC(=C(O4)C=C1)Cl)O)NC7=O)C(=O)O)CC(=O)N)NC(=O)C(C(C)C)NC)O)Cl)O)O)(C)N)O</chem>	CID:14969

(continued)

Table 1. Continued.

S.No	Drug name	Molecular formula	Molecular weight	Structure	SMILES ID	PubChem ID
9	Trimethoprim	C ₁₄ H ₁₈ N ₄ O ₃	290.32 g/mol		<chem>COC1=CC(=CC(=C1OC)OC)CC2=CN=C(N=C2N)N</chem>	CID:5578
10	Doxorubicin	C ₂₇ H ₂₉ NO ₁₁	543.5 g/mol		<chem>CC1C(CC(O1)OC2CC(CC3=C2C(=C4C(=C3O)C(=O)C5=C(C4=O)C(=CC=C5)OC)O)(C(=O)CO)O)N)O</chem>	CID:31703
11	Artemisinin	C ₁₅ H ₂₂ O ₅	282.33 g/mol		<chem>CC1CCC2C(C(=O)OC3C24C1CCC(O3)(O04)C)C</chem>	CID:68827

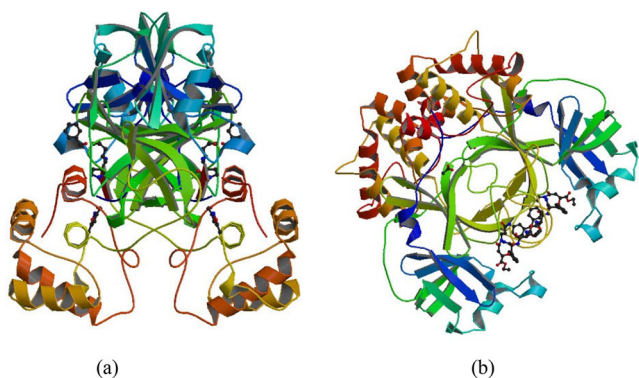


Figure 1. (a) The 3D crystal structure of COVID-19 main protease in complex with an inhibitor N3 (PDB: 6LU7) (Jin et al., 2020) and (b) 3D crystal structure of SARS coronavirus main peptidase (PDB: 2GTB) (with an additional Ala at the N-terminus of each protomer) inhibited by an aza-peptide epoxide (Lee et al., 2007).

from the published structures and CHARMM force field applied for energy minimization (Brooks et al., 2009) using Discovery Studio Visualizer 2019 (Biovia et al., 2000). Also, we have analyzed the active site of the pre-bound ligand molecules in both structures. Furthermore, the active site of each receptor was identified by considering the active site of the inhibitor crystallized with the proteins, for instance, selected all atoms/bonds of any residue in selection zone of within <5 Å and obtained the amino acid residues information available in the active site to implement docking analysis on the same binding pocket. For all the structural visualization, Discovery Studio Visualizer 2019 (Biovia et al., 2000) was used.

2.3. In silico interaction analysis

MGL tool Autodock 4.2 tools protocols were used to predict the interaction energies between drug compounds and

COVID-19 proteins. Interaction analysis was executed through the Lamarckian genetic algorithm (LGA). AutoDock calculate the ligand and receptor interaction binding energy (ΔG) on the basis of the following formula:

$$\Delta G_{\text{binding}} = \Delta G_{\text{gauss}} + \Delta G_{\text{repulsion}} + \Delta G_{\text{hbond}} + \Delta G_{\text{hydrophobic}} + \Delta G_{\text{tors}}$$

Here, ΔG_{gauss} : attractive term for dispersion of two gaussian functions, $\Delta G_{\text{repulsion}}$: square of the distance if closer than a threshold value, ΔG_{hbond} : ramp function – also used for interactions with metal ions, $\Delta G_{\text{hydrophobic}}$: ramp function, ΔG_{tors} : proportional to the number of rotatable bonds (Morris et al., 1998).

Furthermore, water (HOH) was removed during editing of native pdb files of the selected 3D structure of COVID-19 proteins, i.e. main protease (PDB: 6LU7) and peptidase (PDB: 2GTB). The hydrogen atoms, Kollman united charges, and the default solvation parameters were added to both proteins. Gasteiger charge is also assigned to the drug compounds. The Grid box was set to cover the maximum part of both proteins and drug compounds (Jamal et al., 2015). The values were set to $60^\circ \times 60^\circ \times 60^\circ$ in the X-, Y- and Z-axis of a grid point. The default grid point spacing was 0.375 Å. Lamarckian Genetic Algorithm (LGA) was used for proteins–drug compounds flexible docking calculations (Morris et al., 2009). The default LGA parameters like population size (ga_pop_size), energy evaluations (ga_num_generation), mutation rate, crossover rate and step size were set to 150, 2,500,000, 27,000, 0.02, 0.8 and 0.2 Å, respectively. The LGA runs were set at 10 runs. After successful execution of docking steps, obtained conformations of selected SARS-CoV-2 proteins and drug complexes were subjected to further analysis and were deeply analyzed for the interaction energy

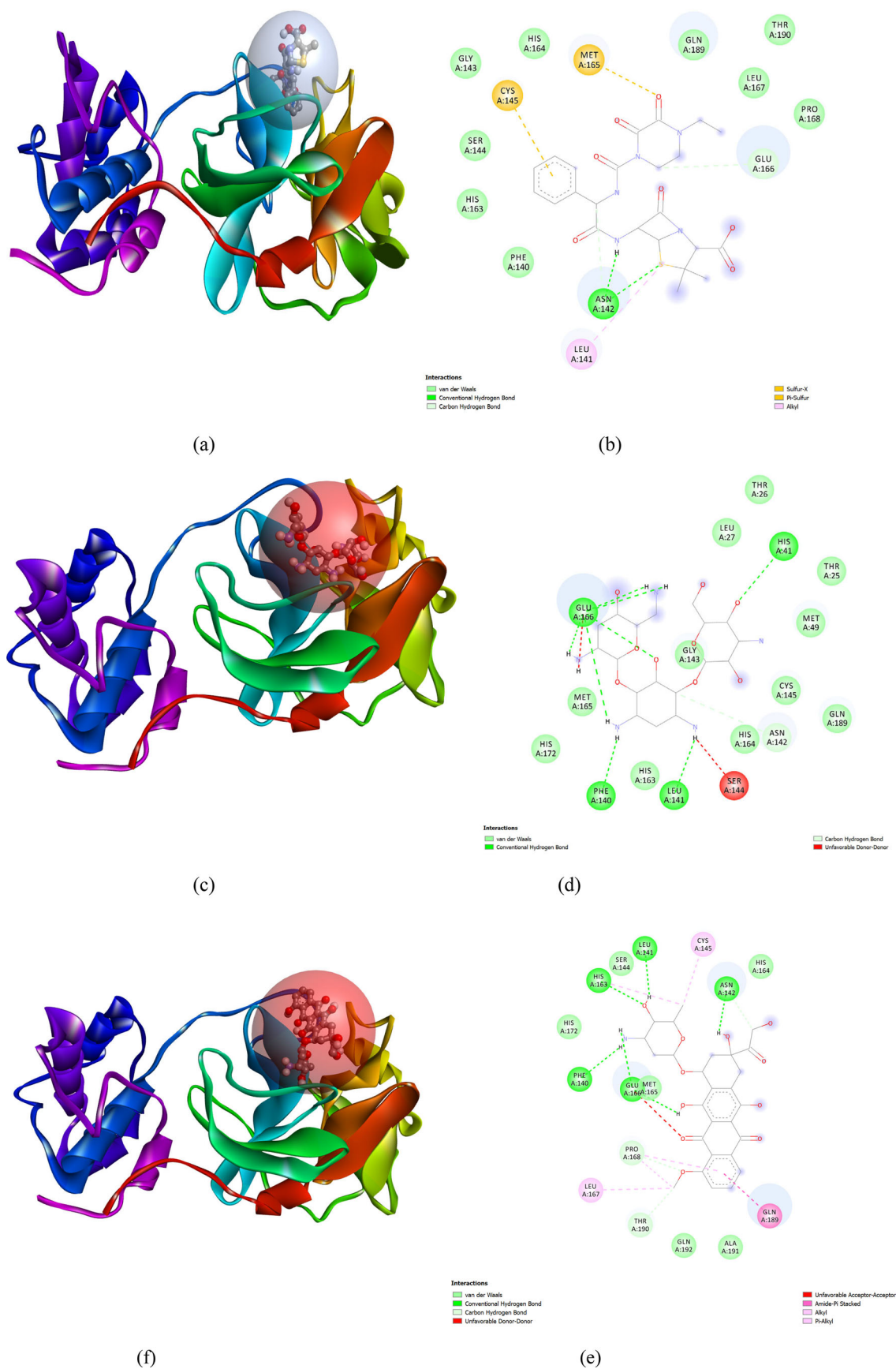


Figure 2. (a,b) Piperacillin, (c,d) tobramycin, (e,f) Doxo (shown by gray color in the sphere with stick pattern) interaction with Covid-19 main protease [shown by rainbow color ribbon pattern (in figures a, c and f)] (PDB: 6LU7). In figures(b, d, e), the surrounding amino acid residues involved in hydrophobic interaction are shown within spheres. Green color dotted lines show the formation of hydrogen bonds. 3D and 2D graphics were generated by Discovery Studio Visualizer 2019.

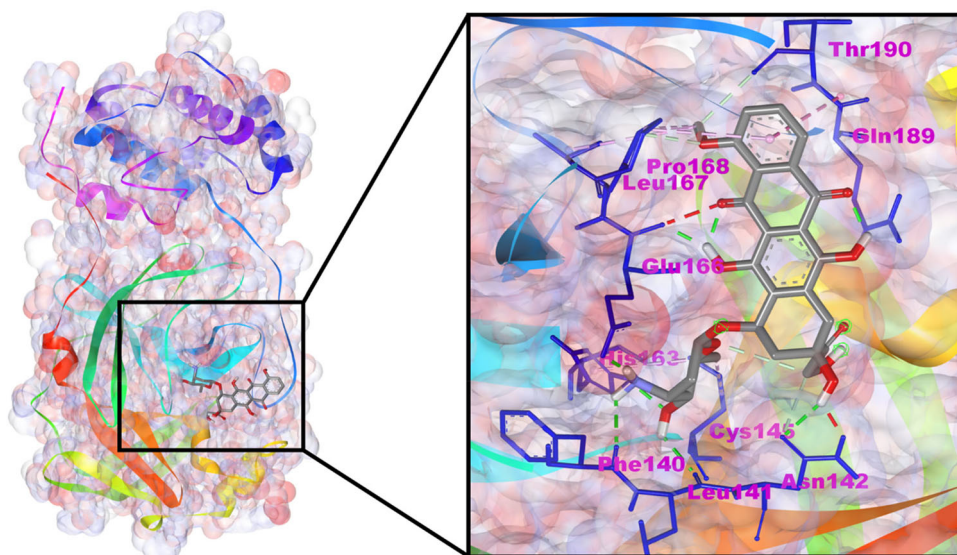


Figure 3. 3D visualization of the binding site of Doxo (in center gray color stick pattern) and interaction with main protease (PDB: 6LU7). Interacting close amino acid residues (shown in blue color with stick pattern) of the binding pocket.

and formation of different types of interactions using Discovery Studio 2019 molecular visualization software.

2.3. MDS experimentation

Doxo–protease and Doxo–peptidase complexes docking results need to be further evaluated through advanced computational techniques. Therefore, the MDS environment was set to execute 100 nanoseconds (ns) simulation using GROningen MACHine for Chemical Simulations (GROMACS) tool 2018 version (Van Der Spoel et al., 2005) developed by the University of Groningen, The Netherlands. Main protease (PDB: 6LU7) simulation in water was performed using GROMACS standard protocol.

For selected complexes simulation initially, pdb2gmx module was used to generate the required main protease (PDB: 6LU7) and peptidase (PDB: 2GTB) topology file followed by CHARMM27 all-atom force field selection. In the next step, ligand (Doxo) topology files were generated from the SwissParam server (Zoete et al., 2011).

For the solvation step, unit cell triclinic box filled with water was created. Na⁺ and Cl[−] ions were added for stabilization of the system leading to the energy minimization execution. Equilibrium setup for the (Doxo–protease complex) system was essential and done followed by two-step ensembles NVT (constant number of particles, volume, and temperature) and NPT (constant number of particles, pressure, temperature). Both ensembles provide control over temperature, pressure coupling resulting in constancy and stabilization of the system through complete simulation (Gupta et al., 2020).

GROMACS contain several packages, for Doxo–protease and Doxo–peptidase complexes MDS analysis, we used gmx rms for root mean square deviation (RMSD) (Kufareva & Abagyan, 2012), gmx rmsf for root mean square fluctuation (RMSF), gmx gyrate for the calculation of radius of gyration (R_g) (Kuzmanic & Zagrovic, 2010) and gmx hbond for the

calculation of numbers of hydrogen-bond formed during the interaction. Finally, after a successful 100 ns simulation run, trajectories files and graphical plots were generated by xmgrace program (Turner, 2005).

2.4. MM-PBSA analysis

The molecular mechanic/Poisson–Boltzmann surface area (MM-PBSA) methods were implemented for the calculation of binding free energy of Doxo–protease and Doxo–peptidase complexes. This calculation validates the extensive analysis of ligand–protein interaction.

The MM-PBSA binding free energies like potential energy, polar and non-polar solvation energies were calculated by the ‘g_mmpbsa’ (Baker, 2001; Kumari et al., 2014) packages using GROMACS. MM-PBSA calculations use the following equation:

$$\Delta G_{\text{binding}} = G_{\text{complex}} - (G_{\text{receptor}} + G_{\text{ligand}})$$

The $\Delta G_{\text{binding}}$ shows the total binding energy of the complex, while the binding energy of the free receptor is G_{receptor} , and that of unbounded ligand is represented by G_{ligand} .

3. Results and discussion

After analyzing molecular interaction results obtained from docking experimentation with selected drugs, we observed that these drugs showed significant interaction efficiency with COVID-19 proteins. Molecular docking results could be evaluated based on final intermolecular energy, inhibition constants and hydrogen bond formation during the interaction between drugs and receptor molecules (Ferreira et al., 2015).

Table 2. Molecular docking results obtained from AutoDock tool simulation run between drug compounds and COVID-19 main protease (PDB: 6LU7).

S. No	Drug name	Final intermolecular energy (kcal/mol)	vdW + Hbond + desolv energy (kcal/mol)	Electrostatic energy (kcal/mol)	Inhibition constant	Hbond name	Hbond length (Å)	Residues involved in hydrophobic interaction
1.	Penicillin	-7.15	-7.07	-0.07	34.65 μ M	A:GLY143:HN- :UNK1:O21 A:GLU166:HN- :UNK1:O12 :UNK1:H30- A:GLN189:OE1 :UNK1:C3- A:ASN142:OD1	2.29382 1.98229 2.14173 3.58787	Leu141, Asn142, Gly143, Ser144, Cys145, His163, His164, Met165, Glu166, Leu167, Pro168, Gln189, Thr190, Gln192
2.	Sulbactam	-5.23	-4.85	-0.38	244.30 μ M	A:GLY143:HN- :UNK1:O14 A:SER144:HG- :UNK1:O11 A:CYS145:HN- :UNK1:O14 A:HIS163:HE2- :UNK1:O11 A:GLU166:HN- :UNK1:O8 :UNK1:H23- A:LEU141:O	2.17265 2.44191 2.72389 1.82619 2.23858 1.66084	His41, Phe140, Leu141, Asn142, Gly143, Ser144, Cys145, His163, His164, Met165, Glu166
3.	Piperacillin	-7.25	-7.56	+0.31	16.49 μ M	A:ASN142:HN- :UNK1:S31 :UNK1:H53- A:ASN142:OD1 :UNK1:C14- A:ASN142:OD1 :UNK1:C5- A:GLU166:O	2.47846 2.09247 3.20829 3.23908	Phe140, Leu141, Asn142, Gly143, Ser144, Cys145, His163, His164, Met165, Glu166, Gln189, Thr190
4.	Tazobactam	-5.55	-5.11	-0.44	110.96 μ M	A:CYS145:HN- :UNK1:O13	2.32432	Thr24, Thr25, Thr26, Leu27, His41, Met49, Asn142, Gly143, Ser144, Cys145, His164, Gln189
5.	Azithromycin	-9.22	-9.00	-0.22	12.43 μ M	A:GLY143:HN- :UNK1:N7 :UNK1:H- A:GLN189:OE1 :UNK1:H- A:ASN142:OD1 :UNK1:C14- A:GLN189:OE1 :UNK1:C42- A:HIS164:O	2.31151 1.98907 2.27374 3.32402 2.84872	Thr25, Thr26, His41, Ser46, Met49, Leu141, Asn142, Gly143, Ser144, Cys145, His164, Met165, Glu166, Leu167, Pro168, Gln189
6.	Ceftriaxone	-7.78	-7.99	+0.21	48.80 μ M	A:THR26:HN- :UNK1:O8 :UNK1:H54- A:HIS164:O :UNK1:H40- A:THR26:O	2.29078 2.37462 1.98039	Thr25, Thr26, Leu27, His41, Met49, Gly143, Ser144, Cys145, His164, Met165, Glu166, Pro168, Arg188, Gln189, Thr190, Gln192
7.	Tobramycin	-9.20	-5.41	-3.79	8.23 μ M	A:HIS41:HE2- :UNK1:O17 A:GLU166:HN- :UNK1:O20 :UNK1:H41- A:LEU141:O :UNK1:H63- A:GLU166:OE1 :UNK1:H64- A:GLU166:OE1 :UNK1:H67- A:GLU166:O :UNK1:H68- A:PHE140:O :UNK1:H69- A:GLU166:OE2 :UNK1:C5- A:ASN142:OD1	2.87136 2.74707 2.18099 2.0668 1.89252 1.91117 2.27924 2.25242 3.79838	Thr25, Thr26, His41, Met49, Phe140, Leu141, Asn142, Gly143, Ser144, Cys145, His163, His164, Met165, Glu166, His172, Gln189
8.	Vancomycin	-4.90	-3.89	-1.01	190.67 μ M	A:THR26:HN- :UNK1:O77 A:HIS41:HE2- :UNK1:O56 :UNK1:H- A:MET165:SD :UNK1:H- A:ASP48:O A:THR25:CA- :UNK1:O77 A:ASN142:CA- :UNK1:O40 A:ASP187:CA- :UNK1:O81	2.42236 3.02627 3.0729 2.45847 3.21739 3.62844 3.77666	Thr24, Thr25, Thr26, Leu27, His41, Val42, Ile43, Cys44, Thr45, Ser46, Asp48, Met49, Leu50, Asn51, Pro52, Tyr54, Leu141, Asn142, Gly143, Cys145, His164, Met165, Glu166, Leu167, Pro168, Phe181, Val186, Asp187, Arg188, Gln189, Thr190, Gln192
9.	Trimethoprim	-6.60	-5.67	-0.93	133.58 μ M	A:HIS163:HE2- :UNK1:N16 :UNK1:H36- A:ASN142:OD1 :UNK1:H38- A:PHE140:O :UNK1:H39- A:GLU166:OE2 :UNK1:C1- A:GLU166:O :UNK1:C10- A:GLU166:O A:GLU166:HN- :UNK1	2.78211 2.12138 1.93292 2.02681 2.92023 3.2576 3.07896	Phe140, Leu141, Asn142, His163, Met165, Glu166, His172, Arg188, Gln189
10.	Doxorubicin	-10.04	-8.42	-1.63	225.44 nM	A:HIS163:HE2- :UNK1:O39 :UNK1:H66- A:PHE140:O :UNK1:H67- A:GLU166:OE2 :UNK1:H68- A:LEU141:O :UNK1:H61- A:GLU166:O :UNK1:H65- A:ASN142:OD1 A:PRO168:CD- :UNK1:O30 :UNK1:C35- A:ASN142:OD1 :UNK1:C31- A:THR190:O	2.17327 2.3384 1.75663 2.08573 1.97082 2.34641 3.01241 3.15293 3.01017	Phe140, Leu141, Asn142, Ser144, Cys145, His163, His164, Met165, Glu166, Leu167, Pro168, His172, Gln189, Thr190, Ala191, Gln192
11.	Artemisinin	-6.94	-6.80	-0.14	8.19 μ M	A:HIS163:HE2- :UNK1:O17 A:GLU166:HN- :UNK1:O9 A:MET165:CA- :UNK1:O18	1.93885 1.79275 3.32272	His41, Phe140, Leu141, Asn142, Gly143, Ser144, Cys145, His163, His164, Met165, Glu166, His172, Gln189

vdW = Van der Waals; Hbond = hydrogen bonds; desolv = desolvation; kcal/mol = kilocalories per molar; μ M = micro molar; nM = nano molar; Å = Angstrom; Hbond name column UNK1 = drug molecule.

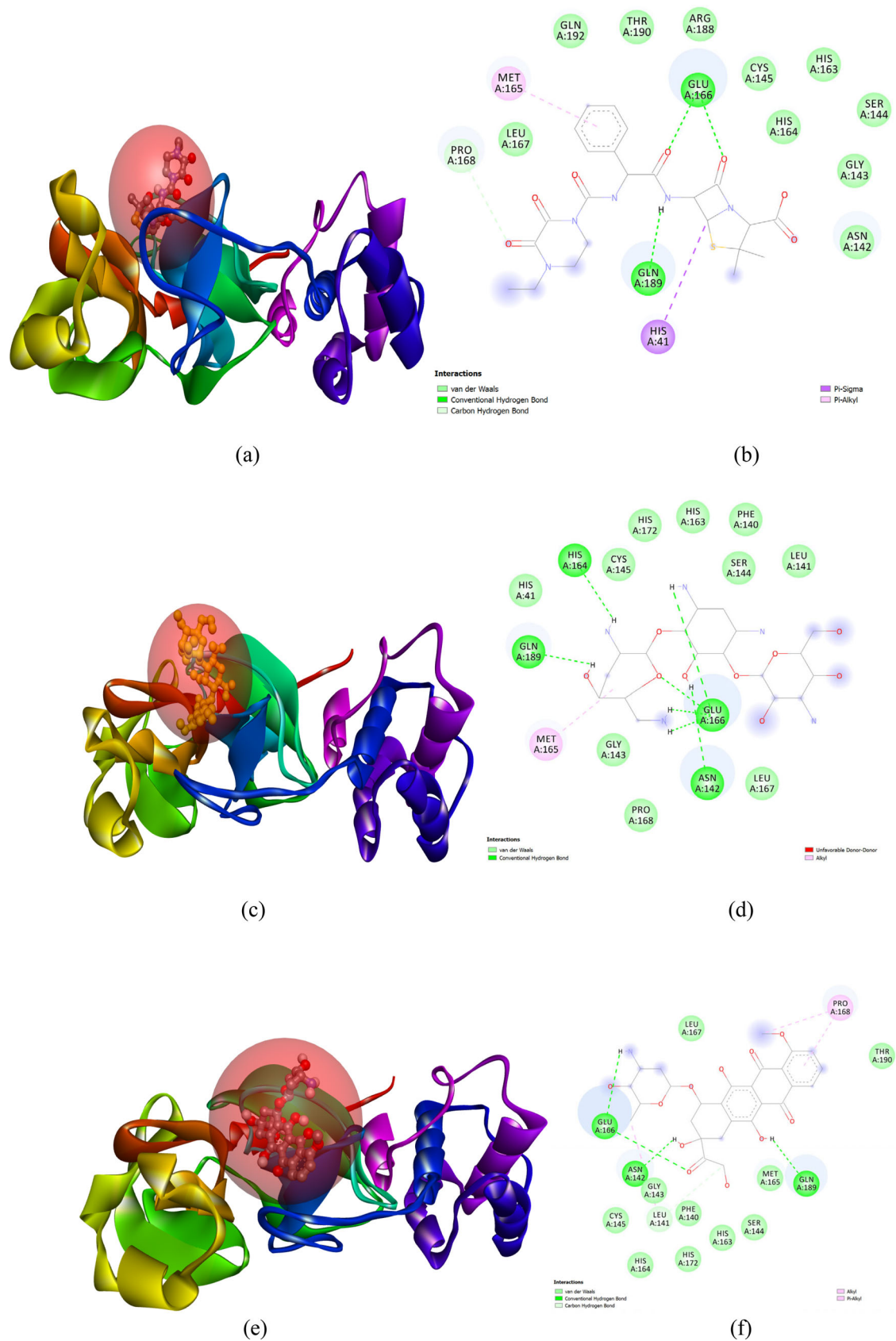


Figure 4. (a,b) Piperacillin, (c,d) tobramycin, (e,f) Doxo (shown by gray color in the sphere with stick pattern) interaction with peptidase [shown by rainbow color ribbon pattern (in figures a, c and f)] (PDB: 6LU7). In figures (b,d,e), the surrounding amino acid residues involved in hydrophobic interaction are shown within spheres. Green color dotted lines show the formation of hydrogen bonds. 3D and 2D graphics were generated by Discovery Studio Visualizer 2019.

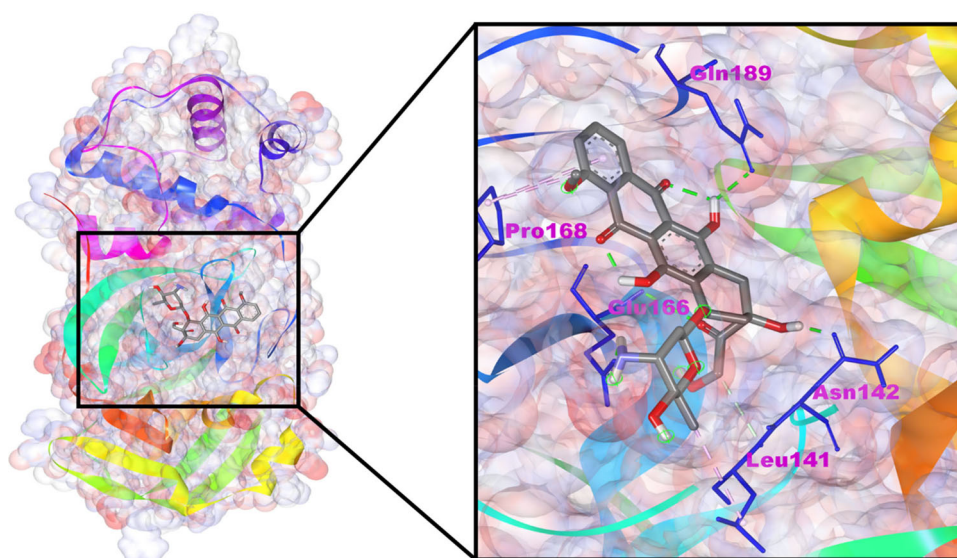


Figure 5. 3D visualization of the binding site of Doxo (in center gray color stick pattern) and interaction with peptidase (PDB: 2GTB). Interacting close amino acid residues (shown in blue color with stick pattern) of the binding pocket.

3.1. Docking analysis with protease (PDB: 6LU7)

Among the docked compounds, piperacillin, tobramycin and Doxo exhibited strong binding with the protease (PDB: 6LU7) than the other compounds. A total of 12 protease residues were found to interact hydrophobically, specifically, Leu141 was found to form alkyl, and a pi-sulfur bond with piperacillin was formed by Cys145 and Met165 (Figure 2(a,b); Table 2), while 16 residues of protease were found to be involved in the interaction with tobramycin in which Leu141, Phe140, Glu166 and His41 formed H bond; His172, Met 165, His163, His164, Asn142, Cys145, Gln189, Met49, Thr25, Thr26, Leu27 were involved in van der waals interaction (Figure 2(c,d); Table 2). Furthermore, Phe140, Leu141, Asn142, Ser144, Cys145, His163, His164, Met165, Glu166, Leu167, Pro168, His172, Gln189, Thr190, Ala191, Gln192 residues of protease were found in the formation of hydrophobic (Gln189 formed amide-pi stacked, Leu167 and Cys145 formed alkyl/pi-alkyl) interaction with Doxo (Figures 2(e,f) and 3; Table 2).

The binding energy and inhibition constant for 'piperacillin–protease', 'tobramycin–protease' and 'Doxo–protease' complexes were found as -7.25 kcal/mol and 16.49 μ M', -9.20 kcal/mol and 8.23 μ M', and -10.04 kcal/mol and 225.44 nM', respectively. Furthermore, the intermolecular energy for the aforementioned complexes was found as -7.25 kcal/mol, -9.20 kcal/mol and -10.04 kcal/mol, respectively.

3.2. Docking analysis with peptidase (PDB: 2GTB)

We have also performed the docking analysis of selected drugs with COVID-19 peptidase (PDB: 2GTB), in which piperacillin, tobramycin and Doxo was found to be strongly bound with COVID-19 peptidase. The observed interaction analysis results have showed that piperacillin interacted with significant binding energy and observed inhibition constant value of were -6.50 kcal/mol and 101.77 μ M, respectively. His41, Asn142, Gly143, Ser144, Cys145, His163, His164, Met165, Glu166, Leu167, Pro168, Arg188, Gln189, Thr190 and Gln192

residues of peptidase were involved in hydrophobic interaction with piperacillin, in which His41 and Met165 have involved Pi-sigma and Pi-alkyl interactions (Figure 4(a,b); Table 3).

Further, His41, Phe140, Leu141, Asn142, Gly143, Ser144, Cys145, His163, His164, Met165, Glu166, His172 and Gln189 residue of peptidase were found to form hydrophobic interaction, specifically Met165 formed alkyl interaction with tobramycin (Figure 4(c,d); Table 3), while Doxo was observed to formed hydrophobic interaction with Phe140, Leu141, Asn142, Gly143, Ser144, Cys145, His163, His164, Met165, Glu166, Leu167, Pro168, Gln189, Thr190 residues of peptidase, in which Pro168 formed alkyl interaction (Figures 4(e,f) and 5). The binding energy and inhibition constant for 'tobramycin–peptidase', and 'Doxo–peptidase' complexes were found as -8.54 kcal/mol and 46.74 μ M', and -9.89 kcal/mol and 451.51 nM', respectively (Table 3). Thus, the interaction energies analyzed from the in silico study against COVID-19 main protease (PDB: 6LU7) with repurposing drugs studied in this study were found to be high [7–8 (<math>4-5.5 kcal/mol)] as compared to previously reported in silico studies with antiviral drugs ritonavir, oseltamivir, remdesivir, ribavirin, chloroquine, hydroxychloroquine, and favipiravir (<math>4-5.5 kcal/mol) (Narkhede et al., 2020).

After analyzing the data (Tables 2 and 3) obtained from the docking analysis, it was found that piperacillin, tobramycin and Doxo drugs could counter COVID-19 protease and peptidase. Thus, from the above results of this study, it was found that Doxo and tobramycin are found to potentiate the inhibition of protease enzyme of the virus. Finally, it is concluded from this study that Doxo showed potential interaction with both viral enzymes protease and peptidase that could be involved to inhibit the pathogenesis of the disease.

3.3. MDS analysis

Furthermore, after MDS total experimentation of 100 ns run, the analysis was done based on obtained data from RMSD,

Table 3. showing molecular docking results obtained from AutoDock tool simulation run between drug compounds and COVID-19 peptidase (PDB: 2GTB).

S.No.	Drugs name	Final intermolecular energy (kcal/mol)	vdW + Hbond + desolv energy (kcal/mol)	Electrostatic energy (kcal/mol)	Inhibition Constant	Hbond Name	Hbond length (Å)	Residues involved in hydrophobic interaction
1.	Penicillin	-6.50	-6.57	+0.07	101.77 μ M	A:GLU166:HN - :UNK1:O12 :UNK1:H30 - A:GLN189:OE1	1.86272 2.3074	His41, Ser144, Cys145, His163, His164, Met165, Glu166, Pro168, Arg188, Gln189, Thr190, Gln192
2.	Sulbactam	-6.01	-5.91	-0.09	67.68 μ M	A:GLN192:HE22 - :UNK1:O7 :UNK1:H23 - A:THR190:O A:PRO168:CD - :UNK1:O11	2.1415 2.07188 3.23096	Met165, Glu166, Leu167, Pro168, Phe185, Val186, Arg188, Gln189, Thr190, Ala191, Gln192, Ala194
3.	Piperacillin	-7.08	-7.26	+0.17	12.70 μ M	A:GLU166:HN - :UNK1:O22 A:GLU166:HN - :UNK1:O28 :UNK1:H53 - A:GLN189:OE1 A:PRO168:CA - :UNK1:O10	2.25634 2.34127 2.35049 3.66374	His41, Asn142, Gly143, Ser144, Cys145, His163, His164, Met165, Glu166, Leu167, Pro168, Arg188, Gln189, Thr190, Gln192
4.	Tazobactam	-6.54	-6.27	-0.27	43.34 μ M	A:GLY143:HN - :UNK1:O13 A:CYS145:HG - :UNK1:O13 A:HIS163:HE2 - :UNK1:N20 A:GLU166:HN - :UNK1:O8 A:HIS172:HE2 - :UNK1:N19 :UNK1:C18 - A:PHE140:O	1.82095 1.9633 1.76011 2.10174 2.74584 3.06169	His41, Phe140, Leu141, Asn142, Gly143, Ser144, Cys145, His163, His164, Met165, Glu166, His172, Gln189
5.	Azithromycin	-5.26	-4.71	-0.55	295.90 μ M	A:GLN189:HE22 - :UNK1:O17 :UNK1:H - A:GLN189:OE1 :UNK1:H81 - A:THR190:O :UNK1:C42 - A:ASN142:OD1 :UNK1:C31 - A:THR190:O	2.56843 2.10966 2.36088 3.57301 3.59106	Asn142, Met165, Glu166, Pro168, Arg188, Gln189, Thr190, Gln192
6.	Ceftriaxone	-7.22	-7.16	-0.06	95.76 μ M	A:GLU166:HN - :UNK1:O35 A:GLN192:HN - :UNK1:O8 :UNK1:H45 - A:GLU166:OE1 :UNK1:H51 - A:PRO168:O :UNK1:H54 - A:GLN189:OE1 :UNK1:C25 - A:GLU166:OE1	2.17687 2.09645 2.0523 1.81608 2.15053 3.47691	Met165, Glu166, Leu167, Pro168, Thr169, Gly170, Gln189, Thr190, Ala191, Gln192, Ala193
7.	Tobramycin	-8.54	-5.91	-2.63	46.74 μ M	A:GLU166:HN - :UNK1:O27 :UNK1:H68 - A:GLU166:OE2 :UNK1:H63 - A:GLU166:O :UNK1:H64 - A:GLU166:O :UNK1:H65 - A:GLN189:OE1 :UNK1:H67 - A:HIS164:O :UNK1:H54 - A:ASN142:OD1	1.95385 2.45744 2.20866 2.25505 1.77835 2.4065 2.6354	His41, Phe140, Leu141, Asn142, Gly143, Ser144, Cys145, His163, His164, Met165, Glu166, His172, Gln189
8.	Vancomycin	-6.08	-5.80	-0.28	180.15 μ M	A:ASN142:HD22 - :UNK1:O8 :UNK1:H35 - A:GLU166:OE1 :UNK1:H41 - A:GLU166:OE1 :UNK1:H48 - A:GLU166:O :UNK1:H33 - A:PRO168:O	2.86481 2.57462 2.56598 2.34308 1.89458	Thr25, Cys44, Met49, Phe140, Asn142, Glu166, Leu167, Pro168, Thr169, Gly170, Gln189, Thr190, Gln192
9.	Trimethoprim	-6.09	-5.27	-0.82	285.15 μ M	A:GLY143:HN - :UNK1:O2 :UNK1:H39 - A:GLU166:OE2 :UNK1:C10 - A:ASN142:OD1	2.6761 2.15739 3.24425	His41, Met49, Phe140, Leu141, Asn142, Gly143, Ser144, Cys145, His163, His164, Met165, Glu166, His172, Gln189
10.	Doxorubicin	-9.89	-8.11	-1.78	451.51 nM	A:GLU166:HN - :UNK1:O34 :UNK1:H66 - A:GLU166:OE1 :UNK1:H65 - A:ASN142:OD1 :UNK1:H54 - A:GLN189:OE1 :UNK1:C35 - A:LEU141:O	2.70445 1.8933 1.88493 2.35702 3.40584	Phe140, Leu141, Asn142, Gly143, Ser144, Cys145, His163, His164, Met165, Glu166, Leu167, Pro168, Gln189, Thr190
11.	Artemisinin	-7.09	-7.08	-0.01	6.40 μ M	A:HIS163:HE2 - :UNK1:O17	2.06985	His41, Phe140, Leu141, Asn142, Gly143, Ser144, Cys145, His163, His164, Met165, Glu166, His172, Gln189

vdW = Van der Waals, Hbond = Hydrogen bonds and desolv = desolvation; kcal/mol = kilocalories per molar; μ M = micro molar; nM = nano molar; Å = Angstrom; Hbond name column UNK1 = drug molecule.

RMSF, R_g and formation of hydrogen bond plots interpretation revealed deviation, fluctuation and stability of main protease, Doxo-protease and Doxo-peptidase complexes during the whole simulation period. The RMSD values for selected simulated molecules was ranged between 0.1 and 0.5 nm (Figure 6(a)). The observed RMSD values for protease, Doxo-protease and Doxo-peptidase complexes were between 0.1 and 0.15 nm, 0.15 and 0.25 nm and 0.1 and

0.5 nm, respectively. In comparison with protease, the Doxo-protease complex showed fluctuation of 40 ns until 55 ns but after that regained stability with an average value 0.25 nm. Although Doxo-peptidase complex was stable until 20 ns but after that shows a sudden increase in the RMSD value, further after 25 ns remained stable until 100 ns (Figure 6(a)). Doxo-protease complex average RMSD value was higher than protease and Doxo-peptidase.

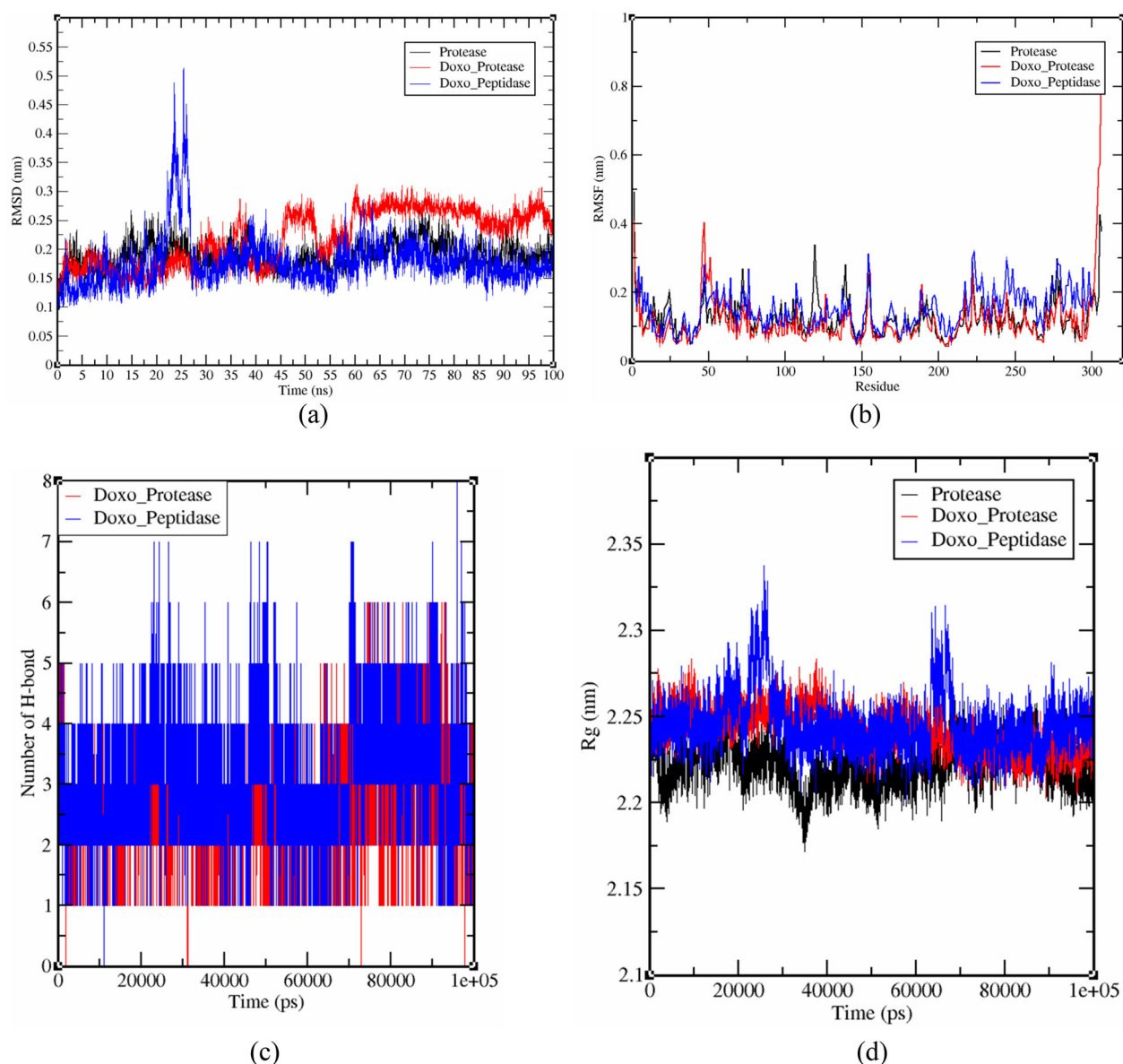


Figure 6. Graphical representation (a) RMSD plot of Main protease (Black color), Doxo–protease (red color) and Doxo–peptidase (blue color) and showing deviation and stability during 100 ns period. (b) RMSF plot with fluctuation per residues. (c) Hydrogen bond plot showing formation hydrogen bonds during 100,000 ps period. (d) Radius of gyration (R_g) plot showing compactness of protease, Doxo–protease and Doxo–peptidase molecule during 100,000 ps simulation, where nm = nanometer; ns = nanosecond; ps = picosecond.

Table 4. List of observed average and standard deviations of all energetic components including the binding energy taken from MM-PBSA analysis.

Complex	Energetic components				
	Van der Waal energy (kJ/mol)	Electrostatic energy (kJ/mol)	Polar solvation energy (kJ/mol)	SASA energy (kJ/mol)	Binding energy (kJ/mol)
Doxo-protease	-119.133 (± 20.298)	-351.951 (± 26.934)	336.804 (± 51.748)	-14.412 (± 1.957)	-148.692 (± 45.697)
Doxo-peptidase	-146.429 (± 28.293)	-323.487 (± 30.927)	382.348 (± 34.897)	-17.799 (± 1.751)	-105.367 (± 21.580)

kJ/mol = kilojoule per mole.

RMSF calculation per residue value was ranged between 0.1 and 0.9 nm for protease, Doxo–protease and Doxo–peptidase complexes and it was observed that for most of the residues RMSF value remains near 0.1 nm for protease and Doxo–protease complex while 0.2 nm for Doxo–peptidase (Figure 6(b)).

Furthermore, few fluctuations were observed at 50–60, 140–170 and 180–210 amino acid residue regions. It shows that amino acid residues at 140–170 and 180–210 regions

are important during Doxo–protease interaction. Amino acid residues present in these regions are also found in the formation of hydrogen bond and hydrophobic interaction during docking analysis (Table 2; Figures 2(f) and 6(b)).

Doxo–peptidase RMSF plot shows fluctuation at 40–50, 140–170, 180–190, 220, 240 and 255 amino acid residue regions. Amino acid residue region 140–170 and 180–190 were involved in the formation of hydrogen bond including hydrophobic interaction (Table 3; Figures 3(f) and 6(b)).

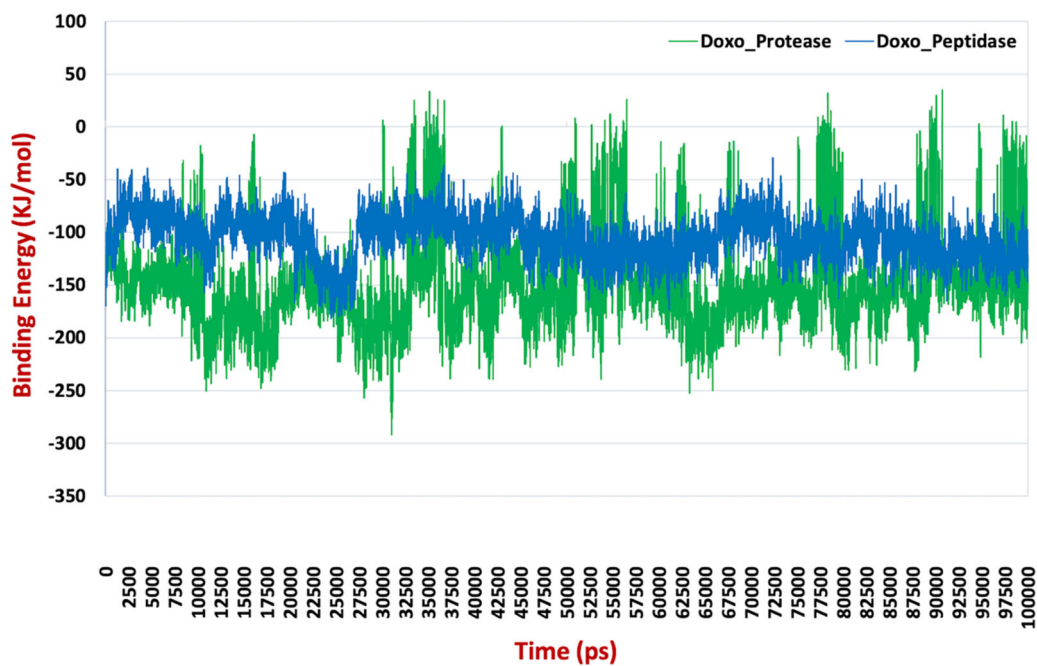


Figure 7. Graph plot showing total predicted MM-PBSA binding energy (kJ/mol) of Doxo–protease (green color) and Doxo–peptidase (blue color) complex interaction during 100,000 ps (100 ns) simulation.

The Doxo–protease and Doxo–peptidase complex hydrogen bond plots shown the formation of 1–6 and 1–8 hydrogen bonds, respectively. Doxo interaction with both SARS-CoV-2 molecules formed 3–4 hydrogen bonds during complete simulation period (Figure 6(c)).

Radius of gyration (R_g) analysis is very important for the assessment of the compactness and stability of protein structure during whole simulation period due to presence of ligand molecules. Main Protease R_g plot has shown average value approximately 2.2 nm. The R_g plot for Doxo–protease and Doxo–peptidase have remained stable and shown average value near to 2.25 nm except few fluctuations found in Doxo–peptidase at 20,000 ps and 60,000 ps. Overall, R_g analysis suggested that both complexes were stable and compactness was maintained for 100,000 ps simulation period (Figure 6(d)).

3.4. MM-PBSA output

Average binding energy and standard deviation were calculated for Doxo–protease and Doxo–peptidase complexes using a script name *MmPbSaStat.py* available in *g_mmpbsa* package (Kuzmanic & Zagrovic, 2010) under GROMACS simulation for Doxo–protease complex interaction (Table 4). Binding energy was obtained after cumulative energies score taken from Van der waal energy, electrostatic energy, polar solvation and solvent-accessible surface area (SASA) energy. All energetic components have shown significant binding score except polar solvation energy. The overall predicted binding energy for Doxo–protease and Doxo–peptidase complexes were $-148.692 (\pm 45.697)$ kJ/mol and $-105.367 (\pm 21.580)$ respectively (Figure 7).

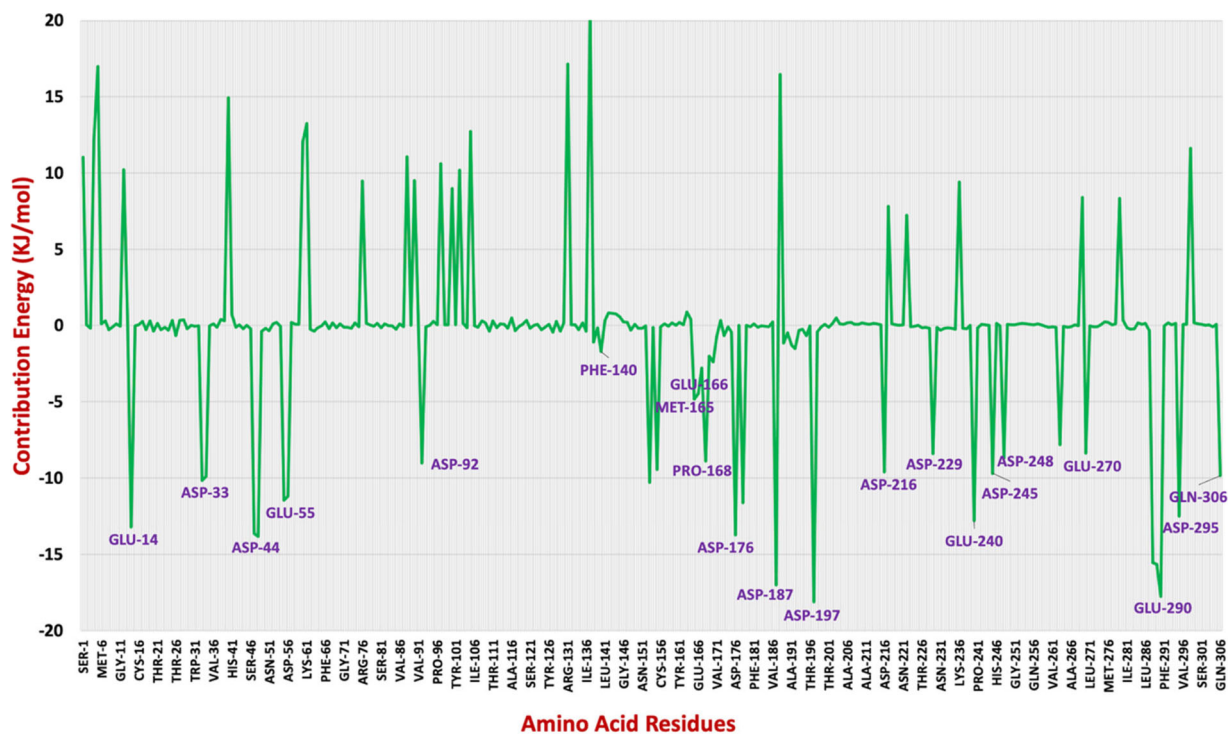
Further, we have also calculated binding energy contribution per residues using a python script *MmPbSaDecomp.py* provided by MM-PBSA package.

After calculation of Doxo–protease interaction contribution energy it was observed that amino acid residues GLU-14, ASP-33, ASP-44, GLU-55, ASP-92, PHE-140, MET-165, GLU-166, PRO-168, ASP-176, ASP-187, ASP-197, ASP-216, ASP-229, GLU-240, ASP-245, ASP-248, GLU-270, GLU-290, ASP-295 and GLN-306 show significant binding affinity (Estrada, 2020). Amino acid residue ASP-197 has shown the most lowest contribution binding energy, i.e. -18.1185 kJ/mol and also amino acid residue ASP-187 has shown -17.0267 kJ/mol contribution energy (Figure 8(a)). Both amino acid residues ASP-187 and ASP-197 have a potential catalytic site and they are important component of S3 subsite of substrate binding loop region 184–197 amino acids of SARS main protease (Gioia et al., 2020; Jin et al., 2020; Zhang et al., 2020; Zheng et al., 2007).

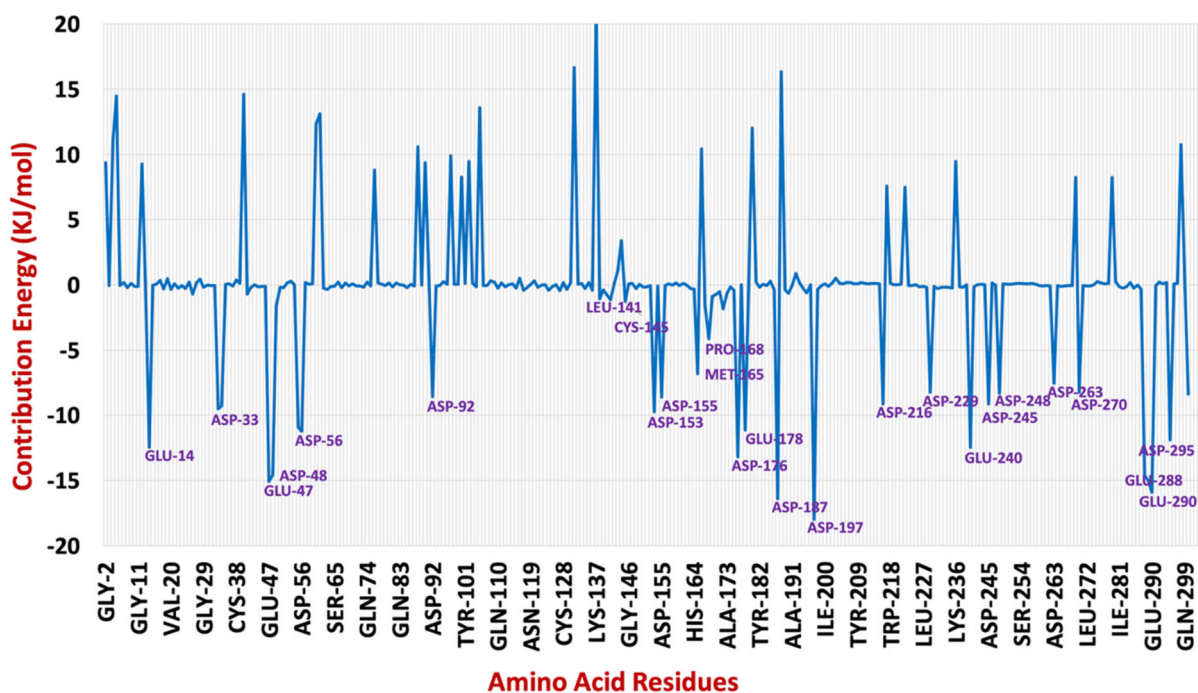
Amino acid residue GLU-166 is a key component. In the protein, generally, N-terminal residues established a hydrogen bond with GLU-166 of the promotor resulting in the shaping of the S1 pocket of the main protease which makes a catalytic pocket (Anand et al., 2002; Zhang et al., 2020). In addition, amino acid residue GLU-166 has shown -4.4742 kJ/mol contribution energy. Contribution energy analysis of Doxo–peptidase interaction plot has shown a similar pattern as Doxo–protease interaction plot. It was observed that ASP-187 and ASP-197 have shown best contribution energies of -16.4063 and -18.007 kJ/mol, respectively (Figure 8(b)). Contribution energy analysis of amino acid residues GLU-166, ASP-187 and ASP-197 revealed that these amino acids played important role during interaction with Doxo which could be established as a repurposed drug against COVID-19 main protease.

4. Conclusions

The interaction energies analyzed from the in silico study against COVID-19 main protease (PDB: 6LU7) and peptidase



(a)



(b)

Figure 8. Graph plot showing calculated binding energy (kJ/mol) contributed by per residues of (a) protease (PDB: 6LU7) and (b) peptidase (PDB:2GTB) during interaction with Doxo.

(PDB:2GTB) with repurposing drug Doxo were found higher than other drugs. Doxo was found to have interacted with the main protease and peptidase significantly. Also, MDS data revealed stability of Doxo–viral biomolecules complexes and MM-PBSA analysis predicted lowest binding free energies.

Thus, the computational studies provided substantial predicted evidence that Doxo could be effective to inhibit the protease-mediated viral entry to the host cell. So, we suggest conducting further in vitro and in vivo antiviral activities of Doxo against the virus to control the COVID-19 disease.

Acknowledgement

The authors are thankful to Qassim University, Saudi Arabia for providing the necessary facilities to conduct the study.

Disclosure statement

The authors declare that there is no conflict of interest.

Ethical approval

Not required

Funding

None

Author contributions

QMSJ and VA did the conceptualization and preparation of original script, designing and execution of methodology. AHA reviewed, edited and prepared the final draft.

ORCID

Qazi Mohammad Sajid Jamal  <http://orcid.org/0000-0001-5525-708X>

Ali H. Alharbi  <http://orcid.org/0000-0003-1815-7287>

Varish Ahmad  <http://orcid.org/0000-0002-6103-0727>

References

- Anand, K., Palm, G. J., Mesters, J. R., Siddell, S. G., Ziebuhr, J., & Hilgenfeld, R. (2002). Structure of coronavirus main proteinase reveals combination of a chymotrypsin fold with an extra alpha-helical domain. *The EMBO Journal*, 21(13), 3213–3224. <https://doi.org/10.1093/emboj/cdf327>
- Ahmad, V. (2020). Prospective of extracellular matrix and drug correlations in disease management. *Asian Journal of Pharmaceutical Sciences*, ISSN 1818–0876, <https://doi.org/10.1016/j.ajps.2020.06.007>. (<https://www.sciencedirect.com/science/article/pii/S181808761931520X>)
- Baker, N. A., Sept, D., Joseph, S., Holst, M. J., & McCammon, J. A. (2001). Electrostatics of nanosystems: application to microtubules and the ribosome. *Proceedings of the National Academy of Sciences of the United States of America*, 98(18), 10037–10041. <https://doi.org/10.1073/pnas.181342398>
- Barretto, N., Jukneliene, D., Ratia, K., Chen, Z., Mesecar, A. D., & Baker, S. C. (2005). The papain-like protease of severe acute respiratory syndrome coronavirus has deubiquitinating activity. *Journal of Virology*, 79(24), 15189–15198. <https://doi.org/10.1128/JVI.79.24.15189-15198.2005>
- Berman, H. M., Westbrook, J., Feng, Z., Gilliland, G., Bhat, T. N., Weissig, H., Shindyalov, I. N., & Bourne, P. E. (2000). The Protein Data Bank. *Nucleic Acids Research*, 28(1), 235–242. <https://doi.org/10.1093/nar/28.1.235>
- Biovia, D. S., Berman, H. M., Westbrook, J., Feng, Z., Gilliland, G., Bhat, T. N., Weissig, H., Shindyalov, I. N., Bourne, P. E., Darden, T., York, D., Pedersen, L. G., Bussi, G., Donadio, D., Parrinello, M., Essmann, U., Perera, L., Berkowitz, M. L., Darden, T., ... Richmond, T. J. (2000). Dassault systèmes BIOVIA, Discovery Studio Visualizer, v. 17.2, San Diego: Dassault Systèmes, 2016. *Journal of Chemical Physics*, 10, 21–9991.
- Brooks, B. R., Brooks, C. L., Mackerell, A. D., Nilsson, L., Petrella, R. J., Roux, B., Won, Y., Archontis, G., Bartels, C., Boresch, S., Cafisch, A., Caves, L., Cui, Q., Dinner, A. R., Feig, M., Fischer, S., Gao, J., Hodoscek, M., Im, W., ... Karplus, M. (2009). CHARMM: The biomolecular simulation program. *Journal of Computational Chemistry*, 30(10), 1545–1614. <https://doi.org/10.1002/jcc.21287>
- Cowan, M. (1999). Plant products as antimicrobial agents. *Clinical Microbiology Reviews*, 12(4), 564–582. <https://doi.org/10.1128/CMR.12.4.564>
- Estrada, E. (2020). Topological analysis of SARS CoV-2 main protease. *Chaos (Woodbury, N.Y.)*, 30(6), 061102 <https://doi.org/10.1063/5.0013029>
- Ferreira, L. G., Dos Santos, R. N., Oliva, G., & Andricopulo, A. D. (2015). Molecular docking and structure-based drug design strategies. *Molecules (Basel, Switzerland)*, 20(7), 13384–13421. <https://doi.org/10.3390/molecules200713384>
- Gioia, M., Ciaccio, C., Calligari, P., De Simone, G., Sbardella, D., Tundo, G., Fasciglione, G. F., Di Masi, A., Di Pierro, D., Bocedi, A., Ascenzi, P., & Coletta, M. (2020). Role of proteolytic enzymes in the COVID-19 infection and promising therapeutic approaches. *Biochemical Pharmacology*, 182, 114225. <https://doi.org/10.1016/j.bcp.2020.114225>
- Gupta, S., Tiwari, N., Verma, J., Waseem, M., Subbarao, N., & Munde, M. (2020). Estimation of a stronger heparin binding locus in fibronectin domain III 14 using thermodynamics and molecular dynamics. *RSC Advances*, 10(34), 20288–20301. <https://doi.org/10.1039/D0RA01773F>
- Huang, C., Wang, Y., Li, X., Ren, L., Zhao, J., Hu, Y., Zhang, L., Fan, G., Xu, J., Gu, X., Cheng, Z., Yu, T., Xia, J., Wei, Y., Wu, W., Xie, X., Yin, W., Li, H., Liu, M., ... Cao, B. (2020). Clinical features of patients infected with 2019 novel coronavirus in Wuhan. *Lancet (London, England)*, 395(10223), 497–506. [https://doi.org/10.1016/S0140-6736\(20\)30183-5](https://doi.org/10.1016/S0140-6736(20)30183-5)
- Jamal, Q. M., Dhasmana, A., Lohani, M., Firdaus, S., Ansari, M. Y., Sahoo, G. C., & Haque, S. (2015). Binding pattern elucidation of NNK and NNAL cigarette smoke carcinogens with NER pathway enzymes: An onco-informatics study. *Asian Pacific Journal of Cancer Prevention*, 16(13), 5311–5317. <https://doi.org/10.7314/apjcp.2015.16.13.5311>
- Jin, Z., Du, X., Xu, Y., Deng, Y., Liu, M., Zhao, Y., Zhang, B., Li, X., Zhang, L., Peng, C., Duan, Y., Yu, J., Wang, L., Yang, K., Liu, F., Jiang, R., Yang, X., You, T., Liu, X., ... Yang, H. (2020). Structure of Mpro from SARS-CoV-2 and discovery of its inhibitors. *Nature*, 582(7811), 289–293. <https://doi.org/10.1038/s41586-020-2223-y>
- Khaerunnisa, S., Kurniawan, H., Awaluddin, R., Suhartati, S., & Soetjipto, S. (2020). Potential inhibitor of COVID-19 main protease (M^{pro}) from several medicinal plant compounds by molecular docking study. Preprints 2020, 2020030226. <https://doi.org/10.20944/preprints202003.0226.v1>
- Kufareva, I., & Abagyan, R. (2012). Methods of protein structure comparison. *Methods in Molecular Biology (Clifton, N.J.)*, 857, 231–257. https://doi.org/10.1007/978-1-61779-588-6_10
- Kumari, R., Kumar, R., & Lynn, A. (2014). g_mmpbsa-a GROMACS tool for high-throughput MM-PBSA calculations. *Journal of Chemical Information and Modeling*, 54(7), 1951–1962. <https://doi.org/10.1021/ci500020m>
- Kuzmanic, A., & Zagrovic, B. (2010). Determination of ensemble-average pairwise root mean-square deviation from experimental B-factors. *Biophysical Journal*, 98(5), 861–871. <https://doi.org/10.1016/j.bpj.2009.11.011>
- Lee, T. W., Cherney, M. M., Liu, J., James, K. E., Powers, J. C., Eltis, L. D., & James, M. N. (2007). Crystal structures reveal an induced-fit binding of a substrate-like Aza-peptide epoxide to SARS coronavirus main peptidase. *Journal of Molecular Biology*, 366(3), 916–932. <https://doi.org/10.1016/j.jmb.2006.11.078>
- Lindner, H. A., Fotouhi-Ardakani, N., Lytvyn, V., Lachance, P., Sulea, T., & Ménard, R. (2005). The papain-like protease from the severe acute respiratory syndrome coronavirus is a deubiquitinating enzyme. *Journal of Virology*, 79(24), 15199–15208. <https://doi.org/10.1128/JVI.79.24.15199-15208.2005>
- Lovato, A., Rossetti, G., & de Filippis, C. (2020). Sore throat in COVID-19: Comment on “Clinical characteristics of hospitalized patients with SARS-CoV-2 infection: A single arm meta-analysis”. *Journal of Medical Virology*, 92(7), 714–715. <https://doi.org/10.1002/jmv.25815>
- Lu, R.-M., Hwang, Y.-C., Liu, I.-J., Lee, C.-C., Tsai, H.-Z., Li, H.-J., & Wu, H.-C. (2020). Development of therapeutic antibodies for the treatment of diseases. *Journal of Biomedical Science*, 27(1), 1–30. <https://doi.org/10.1186/s12929-019-0592-z>

- Lu, S., Lin, J., Zhang, Z., Xiao, L., Jiang, Z., Chen, J., Hu, C., & Luo, S. (2021). Alert for non-respiratory symptoms of coronavirus disease 2019 patients in epidemic period: A case report of familial cluster with three asymptomatic COVID-19 patients. *Journal of Medical Virology*, 93(1), 518–521. <https://doi.org/10.1002/jmv.25776>
- Morris, G. M., Goodsell, D. S., Halliday, R. S., Huey, R., Hart, W. E., Belew, R. K., & Olson, A. J. (1998). Automated docking using a Lamarckian genetic algorithm and an empirical binding free energy function. *Journal of Computational Chemistry*, 19(14), 1639–1662. [https://doi.org/10.1002/\(SICI\)1096-987X\(19981115\)19:14<1639::AID-JCC10>3.0.CO;2-B](https://doi.org/10.1002/(SICI)1096-987X(19981115)19:14<1639::AID-JCC10>3.0.CO;2-B)
- Morris, G. M., Huey, R., Lindstrom, W., Sanner, M. F., Belew, R. K., Goodsell, D. S., & Olson, A. J. (2009). AutoDock4 and AutoDockTools4: Automated docking with selective receptor flexibility. *Journal of Computational Chemistry*, 30(16), 2785–2791. <https://doi.org/10.1002/jcc.21256>
- Narkhede, R., Cheke, R., Ambhore, J., & Shinde, S. (2020). The molecular docking study of potential drug candidates showing anti-COVID-19 activity by exploring of therapeutic targets of SARS-CoV-2. *EJMO*, 4(3), 185–195. <https://doi.org/10.14744/ejmo.2020.31503>
- Pal, M., Berhanu, G., Desalegn, C., & Kandi, V. (2020). Severe acute respiratory syndrome Coronavirus-2 (SARS-CoV-2): An update. *Cureus*, 12(3), e7423. <https://doi.org/10.7759/cureus.7423>
- Pan, S. Y., Zhou, S. F., Gao, S. H., Yu, Z. L., Zhang, S. F., Tang, M. K., Sun, J. N., Ma, D. L., Han, Y. F., Fong, W. F., & Ko, K. M. (2013). New perspectives on how to discover drugs from herbal medicines: CAM's outstanding contribution to modern therapeutics. *Evidence-Based Complementary and Alternative Medicine*, 2013, 627375. <https://doi.org/10.1155/2013/627375>
- Paraskevis, D., Kostaki, E. G., Magiorkinis, G., Panayiotakopoulos, G., Sourvinos, G., & Tsiodras, S. (2020). Full-genome evolutionary analysis of the novel corona virus (2019-nCoV) rejects the hypothesis of emergence as a result of a recent recombination event. *Infection, Genetics and Evolution*, 79, 104212. <https://doi.org/10.1016/j.meegid.2020.104212>
- Shereen, M. A., Khan, S., Kazmi, A., Bashir, N., & Siddique, R. (2020). COVID-19 infection: Origin, transmission, and characteristics of human coronaviruses. *Journal of Advanced Research*, 24, 91–98. <https://doi.org/10.1016/j.jare.2020.03.005>
- Singhal, T. (2020). A review of coronavirus disease-2019 (COVID-19). *Indian Journal of Pediatrics*, 87(4), 281–286. <https://doi.org/10.1007/s12098-020-03263-6>
- Turner, P. (2005). *XMGRADE, Version 5.1*. 19. Center for Coastal and Land-Margin Research, Oregon Graduate Institute of Science and Technology.
- Ullrich, S., & Nitsche, C. (2020). The SARS-CoV-2 main protease as drug target. *Bioorganic & Medicinal Chemistry Letters*, 30(17), 127377. <https://doi.org/10.1016/j.bmcl.2020.127377>
- Van Der Spoel, D., Lindahl, E., Hess, B., Groenhof, G., Mark, A. E., & Berendsen, H. J. (2005). GROMACS: Fast, flexible, and free. *Journal of Computational Chemistry*, 26(16), 1701–1718. <https://doi.org/10.1002/jcc.20291>
- WHO. (2008). *International health regulations (2005)*. World Health Organization.
- Yan, Y., Chang, L., & Wang, L. (2020). Laboratory testing of SARS-CoV, MERS-CoV, and SARS-CoV-2 (2019-nCoV): Current status, challenges, and countermeasures. *Reviews in Medical Virology*, 30(3), e2106. <https://doi.org/10.1002/rmv.2106>
- Zhang, L., Lin, D., Sun, X., Curth, U., Drosten, C., Sauerhering, L., Becker, S., Rox, K., & Hilgenfeld, R. (2020). Crystal structure of SARS-CoV-2 main protease provides a basis for design of improved α -ketoamide inhibitors. *Science (New York, N.Y.)*, 368(6489), 409–412. <https://doi.org/10.1126/science.abb3405>
- Zheng, K., Ma, G., Zhou, J., Zen, M., Zhao, W., Jiang, Y., Yu, Q., & Feng, J. (2007). Insight into the activity of SARS main protease: Molecular dynamics study of dimeric and monomeric form of enzyme. *Proteins*, 66(2), 467–479. <https://doi.org/10.1002/prot.21160>
- Zhou, Y., Hou, Y., Shen, J., Huang, Y., Martin, W., & Cheng, F. (2020). Network-based drug repurposing for novel coronavirus 2019-nCoV/SARS-CoV-2. *Cell Discovery*, 6(1), 14. <https://doi.org/10.1038/s41421-020-0153-3>
- Zoete, V., Cuendet, M. A., Grosdidier, A., & Michielin, O. (2011). SwissParam: A fast force field generation tool for small organic molecules. *Journal of Computational Chemistry*, 32(11), 2359–2368. <https://doi.org/10.1002/jcc.21816>
- Zumla, A., Chan, J. F., Azhar, E. I., Hui, D. S., & Yuen, K. Y. (2016). Coronaviruses – Drug discovery and therapeutic options. *Nature Reviews. Drug Discovery*, 15(5), 327–347. <https://doi.org/10.1038/nrd.2015.37>